DOI: 10.13009/EUCASS2023-637
Aerospace Europe Conference 2023 – 10TH EUCASS – 9TH CEAS

Cold flow analysis of spray angle and droplet size distribution of a pintle injector for green hypergolic propellants

Philipp Teuffel[⋆†], *Lukas Werling*[⋆], *Felix Lauck*[⋆], *Christoph Kirchberger*[⋆]
[⋆]*German Aerospace Center*
Im Langen Grund, 74239 Hardthausen, Germany
philipp.teuffel@dlr.de · lukas.werling@dlr.de · felix.lauck@dlr.de · christoph.kirchberger@dlr.de
[†]Corresponding author

Abstract

In this paper, the effects of spray angle and droplet size for green hypergolic propellants in an initial cold flow investigation using a pintle injector is described. Therefore, simulants were used to match the rheological properties of the propellant combination. The spray was monitored by a shadowgraph setup and measured by a droplet size measurement system. With shadowgraph measurements the spray cone angle was determined and compared to previous research literature. First insights of the influence of high viscous fluids on droplet size distribution from pintle injectors could be gained. Results indicate that the viscosity has a minor influence on the spray angle but larger impact on droplet size.

1. Introduction

Over the past few decades, pintle injectors have proven themselves for throttling applications in rocket engines [1]. Here, often hydrazine-based propellant combinations were successfully used [2]. Because of high efforts in the space sector to substitute hydrazine and its derivates by green propellants, not only new propellants with competitive properties must be found but also new rocket elements like injectors, combustion chambers or valves must be developed. One promising substitute for hydrazine-based propellant combinations is based on ionic liquids as fuel and hydrogen peroxide as oxidizer. In earlier research by Negri and Lauck [3] a green hypergolic propellant combination called HIP_11 is presented. This combination is based on the ionic liquid 1-ethyl-3-methylimidazolium thiocyanate (EMIM SCN) and of 97 wt.-% high test peroxide (HTP). Additionally, copper thiocyanate (Cu SCN) is added to the ionic liquid in order to accelerate the hypergolic ignition. In drop tests with this propellant combination ignition delay times lower than 20 ms were measured [4]. Further, the theoretical specific impulse is also comparable to traditional hypergolic propellant combinations, e. g. monomethylhydrazine (MMH) and nitrogen tetroxide (NTO). The maximum specific impulse can be reached at oxidizer to fuel ratio (ROF) of about 3.9. Additionally, the rheological parameters of the ionic liquid differ from hydrazine-based fuels which requires new injector designs. Predominantly, the ionic liquid has a higher viscosity than MMH.
Pintle injectors are not only capable to throttle but also combine the benefits of a proper impingement between the propellants and a formation of an uniform spray cone. Nevertheless, designing a pintle injector for green hypergolic propellants can be challenging due to their higher viscosities and higher ROF compared to conventional hypergolic propellants. Also, less design guidelines are available in open literature. One important design criterion is the total momentum ratio (TMR), which is defined by [5]

$$TMR = \frac{\dot{m}_\mathrm{i} \cdot v_\mathrm{i}}{\dot{m}_\mathrm{o} \cdot v_\mathrm{o}}. \tag{1}$$

Here, $\dot{m}$ indicates the mass flow and v the exit velocity of the fluids. The subscript i indicates the here called inner fluid which goes through the pintle and leaves the pintle tip radially. The subscript o indicates the here called outer fluid, which goes in axial direction in an annular stream along the outer pintle surface. It is claimed that optimal performance can be reached at $TMR = 1$ [5]. Besides that, the resulting spray angle after impinging of radial and axial stream depends on the momentum ratio. With a high TMR, the spray cone angel becomes larger, whereas with low TMR the spray cone angle gets narrower. In open literature, the spray cone angle of liquid-liquid pintle injectors is investigated. Cheng et al. [6] conducted a numerical simulation to predict the spray cone angle and compare the results to experiments. The pintle injector shows a continuous slit with a 90° liquid sheet impingement. They derived a formula for the half spray cone angle φ of a liquid-liquid pintle injector [6]

DOI: 10.13009/EUCASS2023-637

$$\cos\varphi = \frac{1}{1 + TMR}. \tag{2}$$

Within this publication, water was used as fluid. Equation 1 and Equation 2 are not dependent on the viscosity. Therefore it is not clear if spray angle or performance of a liquid-liquid pintle injector are influenced when used with fluids of a different viscosity. In addition, database is limited regarding droplet size measurement for the liquid-liquid pintle injection with higher viscous fluids.

Besides few guidelines for pintle injector designs compared to e.g. swirl injectors, in publications often only low viscous propellant simulants like water were used. In general, more design guidelines in open literature are needed to develop suitable pintle injectors in the future. That is even more inevitable if new propellant combinations with different properties come into place. In order to develop proper pintle injectors for green hypergolic propellants, the influence of viscosity on the spray behaviour must be investigated. Additionally, changing operation conditions of the propellant combination complicate the direct transfer of conventional injector hardware to new challenges. Addressing the challenges mentioned above, initial results of cold flow tests of a pintle injector are presented in this paper. The spray of water and glycerin based simulants were recorded by using a shadowgraph setup. From the shadowgraph images the spray cone angle was measured and compared between the different simulant injection tests as well as to literature. Furthermore, the droplet size distribution is compared between the two simulant combinations.

2. Pintle injector design

In the past, a lot of different designs and geometries of pintle injectors have been developed, tested and are operating successfully. However, this design knowledge and iterative development procedure remains often unpublished within the institutions.

2.1 Challenges

Multiple challenges come up when designing and calculating pintle injectors for green hypergolic propellant combinations. A major drawback is that pintle injectors had been working predominantly with hydrazine-based propellants. Based on the big difference in rheological and performance behaviour, it is not possible to use similar injection geometries like with hydrazine-based pintle injectors. In Table 1 is a comparison between some important parameters when it comes to injection and performance.

Table 1: Comparison of injection related properties between MMH/NTO and EMIM SCN/H_2O_2

	Density in $\frac{kg}{m^3}$	**Dynamic viscosity** in mPas	**Surface tension** in $\frac{mN}{m}$	**ROF** at max. I_{sp}	**Literature** –
MMH	880	0.85	33.50	≈ 1.65	[7]
NTO	1450	0.42	26.50		
EMIM SCN[a]	1110	20.1	46.30	≈ 3.9	[4]
H_2O_2[b]	1425[a]	1.256	79.90		[8]

[a] at 298 K
[b] at 293 K

By comparing the rheological properties of the fuels MMH and EMIM SCN the much higher viscosity of the ionic liquid is clearly visible. This higher viscosity makes atomization much more difficult compared to the lower viscous MMH. In addition, the ROF plays an important role in pintle injector design, too. Form Equation 1 it is visible that the TMR depends on ROF. As suggested in literature, TMR should be close to 1 for best performances [5]. To confirm this statement, the fluid exit velocity ratio in Equation 1 must be the reciprocal value of the ROF. This means that with high ROF like the green propellants, the oxidizer has a much smaller injection velocity than the fuel. For hypergolic propellant combinations the injection velocity is of high importance when it comes to ignition and combustion. Phenomenons like reactive sheet or jet separation and combustion chamber fluctuations can occur and need to be avoided. Additionally, with the high viscosity of the fuel even a higher pressure drop over the injector is needed to accelerate the fuel to the required flow velocities. Lastly, injector design and combustion chamber design need to provide a fast, smooth and reliable ignition of the green hypergolic propellant.

DOI: 10.13009/EUCASS2023-637

2.2 Design

The pintle injector tested and presented in this paper is shown in Figure 1. The aim of this injector development was to reduce the functionality of the different pintle injector designs from literature to a basic functionality concept. This basic functionality concept includes a 90° liquid sheet impingement at the exit of the inner fluid to create an uniform spray cone. The injector is designed only for cold flow testing.

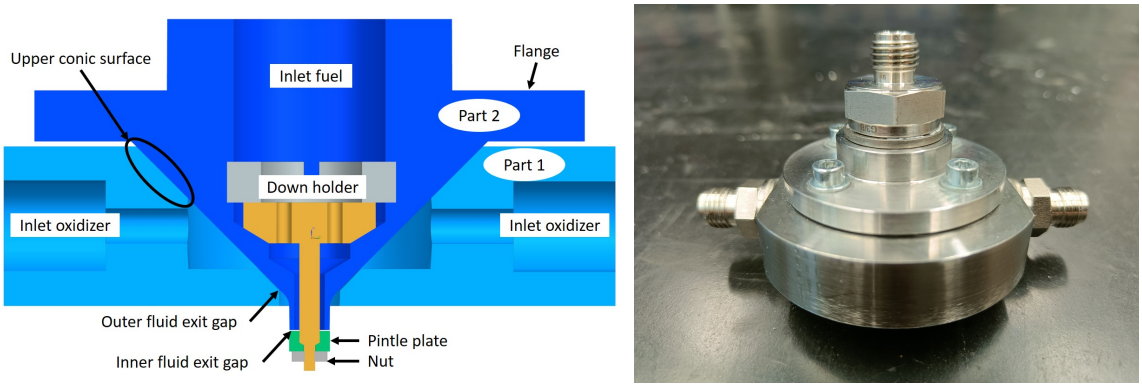

Figure 1: Simplified liquid-liquid pintle injector, left: Cross section of the injector model, right: Tested pintle injector assembly

The injector consists of two main parts (part 1 and part 2) which are connected by a flange. The conical parts 1 and 2 are pressed into each other and have contact with the upper conic surface. At the outer fluid exit gap, the conic of part 1 is slightly larger than at the upper part. Due to the constant conical shape of part 2, a gap between part 1 and part 2 at the outer fluid exit gap is formed. With this arrangement the outer fluid exit gap can be manufactured very precisely. The distributor ring for the outer fluid has inlets from two sides to generate an uniform injection pressure distribution. The outer fluid flows along the pintle to the inner fluid exit gap, where impingement takes place. The inner fluid has one inlet. Through a slit the fluid leaves the pintle tip radially. The pintle plate, which is fixed with a nut, forms the inner fluid exit gap. In this concept also no direct seals between fuel and oxidizer are necessary.
It was contemplated to design a pintle injector for a 200 N green hypergolic propellant thruster. The design of the necessary cross section areas at the exit of both fluids were set to the restrictions of the in-house manufacturing tolerances. The heights of the inner and outer gaps are 0.1 mm. With the pressure loss equation

$$\dot{m} = C_\mathrm{d} A \sqrt{2\rho\Delta p} \tag{3}$$

the mass flow rate $\dot{m}$ was estimated. Here, C_d indicates the discharge coefficient, A the cross section area of the fluid exit gap, ρ the density of the fluid and Δp the pressure loss over the injection geometry. Due to few liquid-liquid pintle injector publications and the great variety of different pintle injector types used, it is hard to estimate C_d values for an own development.

3. Cold flow test bench

An important element of a successful rocket engine operation is the injector. The design of injector elements can be challenging due to their complexity. Designing and creating injector elements for new applications usually needs several iterations before satisfying results are achieved. Before testing injector elements in hot firing tests, developers can get initial ideas of the performance of their injectors through cold flow testing. Instead of using the propellants itself, simulants are used to evaluate the spray behaviour. Also, cold flow tests can reduce costs in the development process of new injectors since iterations of new developments can be realized faster. Therefore, a new cold flow test bench was built at DLR test bench M11 to investigate injector elements. The test bench set up is shown in Figure 2. Two separate tanks are used for fuel and oxidizer simulants. Both tanks can be pressurized independently by PID-controlled pressure regulators. Within the fluid lines temperature, pressure and mass flow rate are measured. Thermocouples of Type K with 1 mm in diameter with an uncertainty of ±1.5 K at a sampling rate of 333 Hz are used for temperature measurements. Piezo-resistive pressure transducers with a measurement range from 0 bar to 20 bar and an uncertainty of about ±0.1 bar at a sampling rate of 1000 Hz are used to measure the absolute pressure. In this paper, the pressure drop over the injector for the inner and outer fluid channel is calculated as the difference between P-5, respectively P-6, and the ambient pressure. The mass flow rate in both fluid lines is measured with Coriolis measurement systems.

DOI: 10.13009/EUCASS2023-637

Coriolis 1 with a measurement range of 0 g/s to 33 g/s is used to measure the mass flow rate of the fuel simulant. Coriolis 2 with a measurement range of 0 g/s to 83 g/s is used to measure the mass flow rate of the oxidizer simulant. A real time measurement system is implemented for precise data acquisition and control. The test bench can be controlled by a Graphical User Interface (GUI), which is realized via Python.

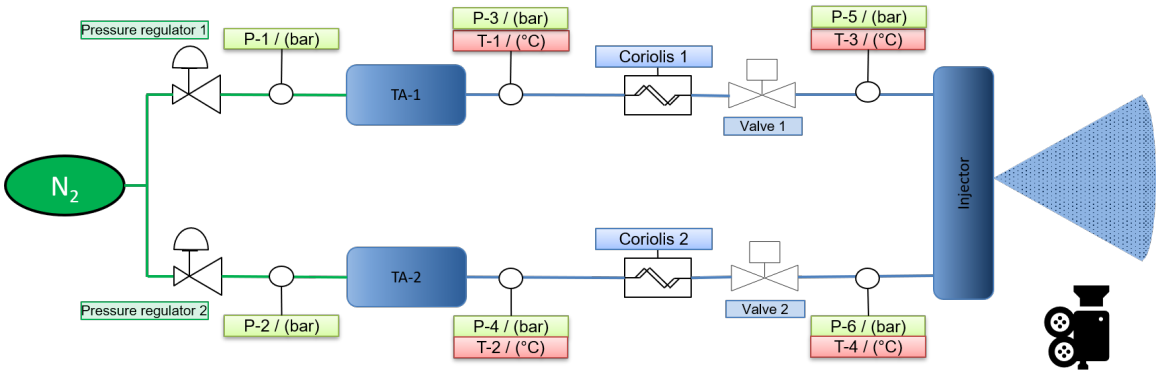

Figure 2: Schematic of the fluid plan at the DLR Cold Flow Test Stand

Additionally, there is a high speed shadowgraph system, a droplet size measurement system and a spray chamber with optical access for spray diagnostic on-site. The shadowgraph system and the droplet size measurement system can be used at ambient conditions but also in combination with the spray chamber. Both measurement systems are triggered with the real time system, hence they are synchronized with the measurement data. This provides a detailed investigation of the spray behaviour.

3.1 Shadowgraph measurement system

The shadowgraph system consists of a high speed camera and a back light. The high speed camera records black and white images at 5000 frames per second with high shutter speed. In front of the backlight is frosted glass in order to realize a consistent illumination and background. From these images the spray cone angle can be measured. In this paper the spray cone angle is measured manually (Figure 3). Therefore, the frames are averaged over the evaluation interval to generate a flatted cone edge. Before every test series, a reference measurement was performed to calibrate the pixel size to a length measurement within the spray. With a distance of 6 mm below the impinging point of the inner and outer fluid, the radial distance from the centre to the cone edge can be measured. Then, the spray angle is calculated with both distances. It must be mentioned that the spray angle may differ when choosing different measurement positions due to non-linear cone edges. By adding the right and left angle of the spray cone, the spray cone angle can be determined.

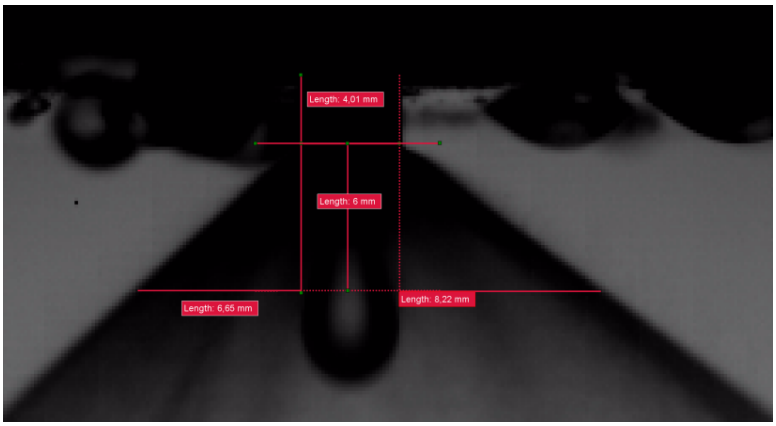

Figure 3: Principle of spray cone angle measurement

DOI: 10.13009/EUCASS2023-637

3.2 Droplet size measurement system

The droplet size distribution was measured with a Spraytec device from Malvern Panalytical GmbH. This measurement system is based on the Mie scattering principle. A He/Ne-Laser is used to generate a parallel beam. The spray was positioned in the middle between laser and detector head. The distance from the impinging point to the centre of the laser beam is about 85 mm. For all tests the refractive index was kept constant.

4. Test results

Every single injection test was performed until stationary conditions for pressure and mass flow rate were achieved (Figure 4). Within this stationary range an evaluation interval of 30 ms was chosen to average the measurement data, the shadowgraph images and droplet size distributions. With a short evaluation interval the averaged shadowgraph frames show a sharper spray cone edge, whereas with longer evaluation intervals and varying conditions the spray cone size changes and the spray cone edge becomes blurry.

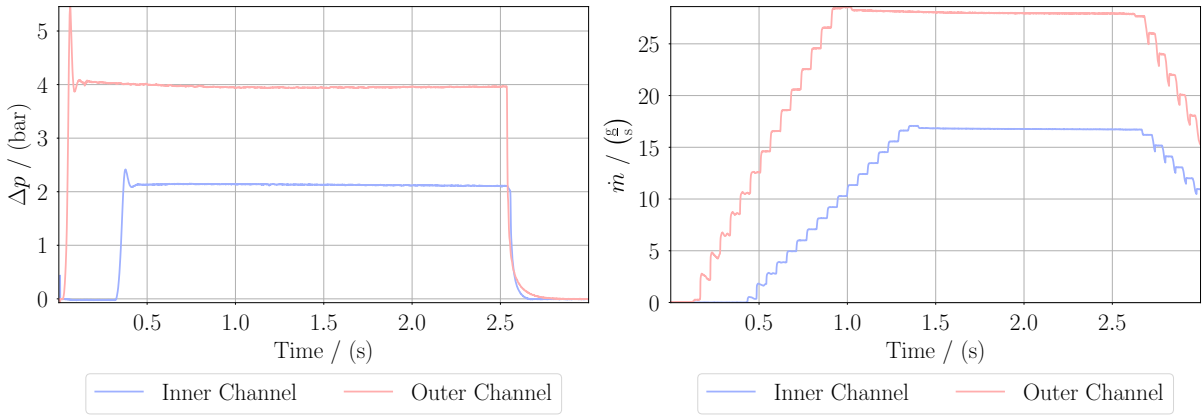

Figure 4: Example of a single injection test, left: pressure drop over injection time, right: mass flow rate over injection time

Before and after the injection tests, the height of the inner fluid exit gap at the pintle tip was measured with a gauge to ensure that the cross section area does not change with higher injection pressures. It was found that the height of the gap at the pintle tip did not change during the tests. The gap for the outer fluid could not be measured due to its inaccessibility. However, the outer gap can be assumed to be much more stable. Between all injection tests the injector was not disassembled to keep the same flow geometries.
Two different test series were conducted. In the first test series shadowgraph recordings were made. In the second test series droplet size measurements were conducted. In both test series, injection tests with different fluid combinations were performed. Firstly, only water was used as simulant for fuel and oxidizer (water/water injection). Secondly, a mixture of glycerol and water was used to simulate the fuel and water was used to simulate the oxidizer (mixture/water injection). In Table 2 are the resulting fluid properties shown. All tests were performed at an ambient temperature of about 285 K and an ambient pressure of 0.98 bar. By comparing the Ohnesorge Number [5]

$$Oh = \frac{\mu}{\sqrt{\rho \sigma D}} \tag{4}$$

of fuel and fuel simulant, respectively oxidizer and oxidiser simulant, it can be seen that the simulants cover the rheological properties of the propellant combination concerning spray behaviour. In Equation 4, μ is the viscosity, ρ is the density, σ is the surface tension and for the characteristic length D the fluid exit gab height of 0.1 mm is used.

4.1 Shadowgraph images

The difference of the spray pattern between water/water injection and mixture/water injection can be seen in Figure 5. In both tests the mass flow rate through the inner and outer channel are at 16 g/s and 20 g/s respectively. It can be seen from the images that by injecting a higher viscous fluid the spray tends to form bigger droplets and ligaments. Additionally, the spray tends to agglomerate into fluid streams along the spray cone.

DOI: 10.13009/EUCASS2023-637

Table 2: Comparison of injection related properties between simulants and EMIM SCN/H_2O_2

	Density in $\frac{kg}{m^3}$	**Dynamic viscosity** in mPas	**Surface tension** in $\frac{mN}{m}$	**Oh** –	**Literature** –
Glycerol / Water (70 wt.% / 30 wt.%)[a]	1185	42.3	67.97	≈ 14.9	[9, 10, 11]
Water[a]	999.51	1.24	73.95	≈ 0.46	[12]
EMIM SCN[b]	1110	20.1	46.30	≈ 8.86	[4]
H_2O_2[c]	1425[b]	1.256	79.90	≈ 0.37	[8]

[a] at 285 K
[b] at 298 K
[c] at 293 K

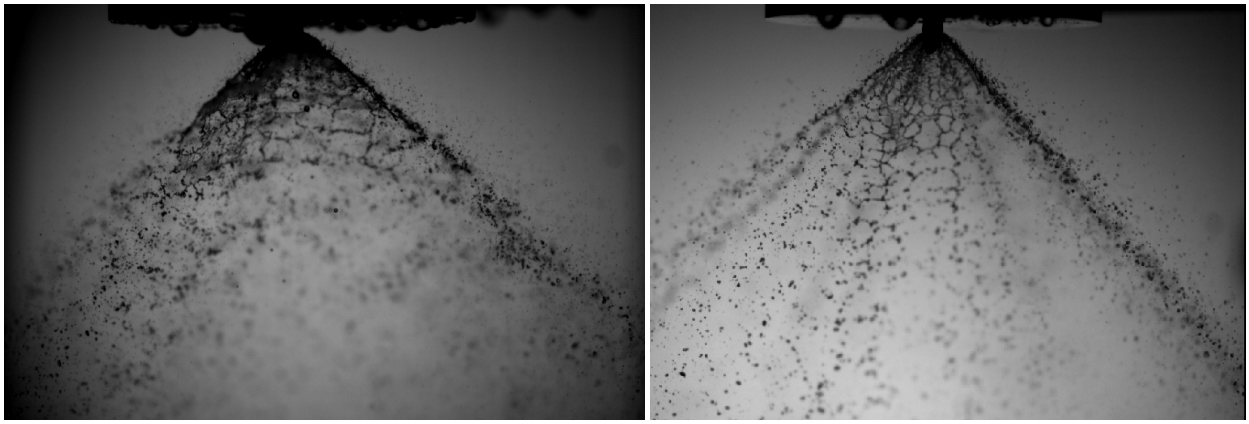

Figure 5: Shadowgraph images of two injection tests, left: water/water injection, right: mixture/water injection

In Figure 6 the resulting mass flow rate over the injector pressure drop for every single injection test averaged over the evaluation interval is shown. Only low pressure drops were tested to not exceed the mass flow range. The graphs show that even with the smallest possible in-house manufacturing tolerances the fluid exit cross section area is large which results in high mass flow rate and low pressure losses.

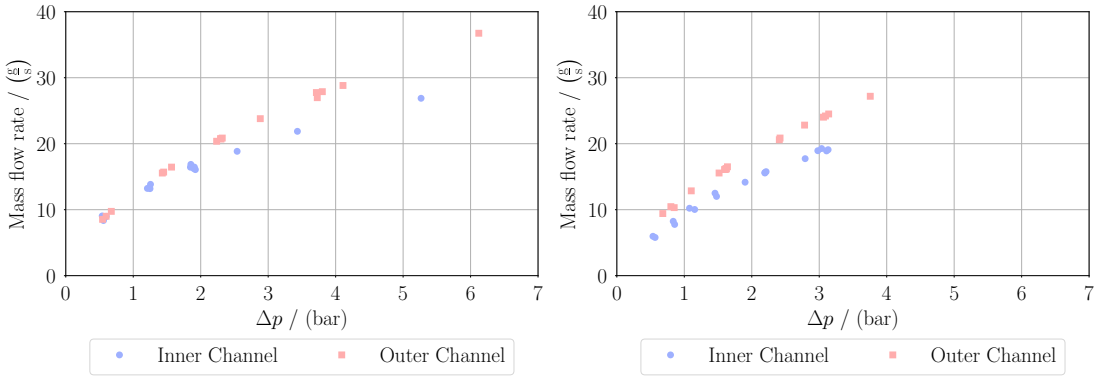

Figure 6: Mass flow rate over pressure drop for all injection tests, left: water/water injection, right: mixture/water injection

The discharge coefficient of the inner and outer fluid channels is shown in Figure 7. The discharge coefficients were calculated with Equation 3. In both diagrams, the discharge coefficient at the outer channel is reproducible. With increasing pressure drop the discharge coefficient at the outer channel becomes constant ($C_d \approx 0.53$). Compared to the outer channel, the discharge coefficient of the inner channel shows a different reaction between water/water and mixture/water injection. With water injection through the inner channel there was a constant discharge coefficient ($C_d \approx 0.67$), whereas with the mixture injection through the inner channel, the discharge coefficient increases with increasing pressure drop. From the data available it seems that the discharge coefficient reaches a constant value at

DOI: 10.13009/EUCASS2023-637

$\Delta p \approx 3$bar of $C_\mathrm{d} \approx 0.56$. It is estimated to have an error of about ± 0.15 for the C_d values, which is manly caused by the uncertainty of the fluid exit gap height measurement.

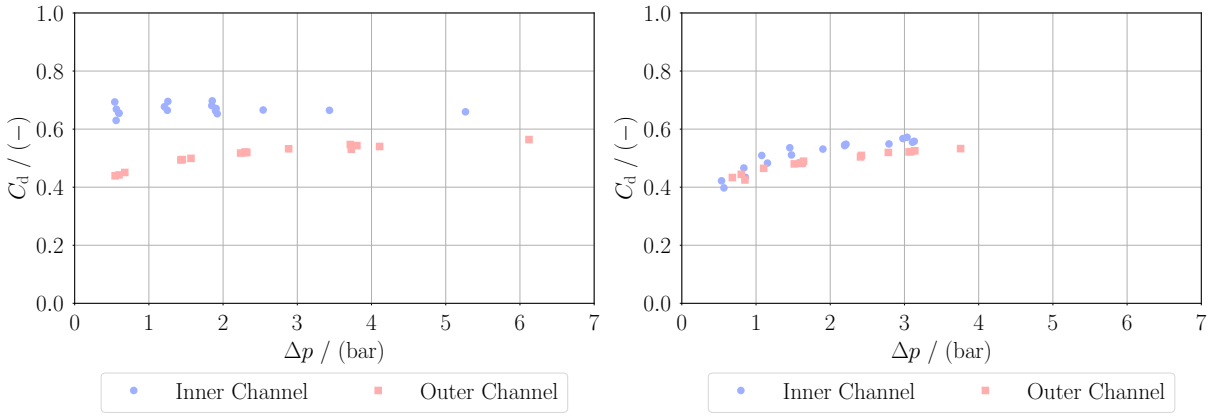

Figure 7: Discharge coefficient over pressure drop for all injection tests, left: water/water injection, right: mixture/water injection

In the left diagram of Figure 7 the discharge coefficient of the inner channel varies at the same pressure drop. This behaviour can be analysed in Figure 8. Here, the discharge coefficient of the inner channel is plotted over the pressure loss of the outer channel with water/water injection. With a constant pressure drop at the inner channel, the discharge coefficient decreases with increasing pressure drop respectively increasing mass flow rate of the outer channel. The flow through the inner channel becomes throttled due to the pressure in the annular outer flow. This influence should be considered when designing pintle injectors. A variation of discharge coefficient at the inner channel could not be seen with mixture/water injection due to small amount of data.

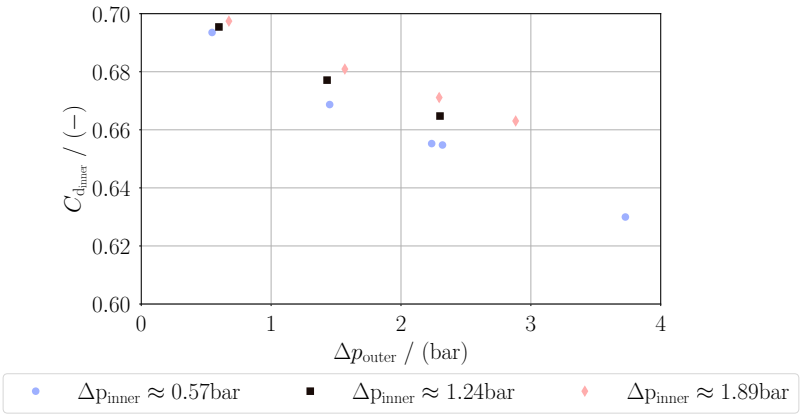

Figure 8: Discharge coefficient of inner channel over pressure drop of outer channel with water/water injection

Figure 9 shows the spray cone angle at different TMR. The spray cone angle is measured as described in Section 3.1 and the TMR is calculated with Equation 1. The dotted line in both graphs represent the spray cone angle from Equation 2, which was found to be comparable to this study. In both diagrams the spray cone angle increases with increasing TMR. Nevertheless, the measured spray cone angle underestimates the model from Cheng et al. [6]. During the cold flow tests it was found that the spray cone is not perfectly uniform in all directions. This can lead to a deviation in the spray angle compared to literature. Furthermore, an error of about $\pm 10°$ for the spray cone angle is estimated by using the descried method in Figure 3. Besides that, the difference in spray cone angle between the two test series is minor. It is noticeable that with the mixture/water injection in four injection tests no spray cone was formed. Hence, even for a wide range of TMR the spray cone angle is 0°.

4.2 Droplet size distribution

In Figure 10 the droplet size distribution of two tests is shown. Both tests have comparable mass flow rates at about 13.5 g/s and 20.0 g/s through the inner and outer channel respectively. The left diagram shows a water/water injection

DOI: 10.13009/EUCASS2023-637

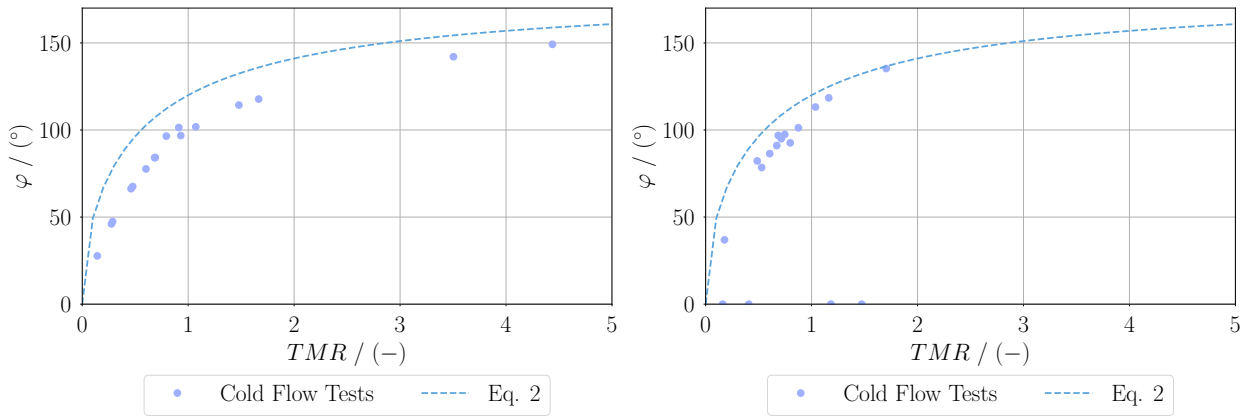

Figure 9: Spray cone angle over TMR, left: water/water injection, right: mixture/water injection

test. The right diagram represents a mixture/water injection test. By comparing the droplet size distribution it is visible that more big droplets are formed with the mixture/water injection. In addition, in Figure 5 two shadowgraph frames from these tests are compared to each other. However, in both tests a similar operating point was achieved and the same injector was used, even though the spray behaviour differs a lot when using a high viscous fluid as fuel. At low pressure levels the shadowgraph images with the high viscous fuel simulant seem to agglomerate fluid into bigger droplets.

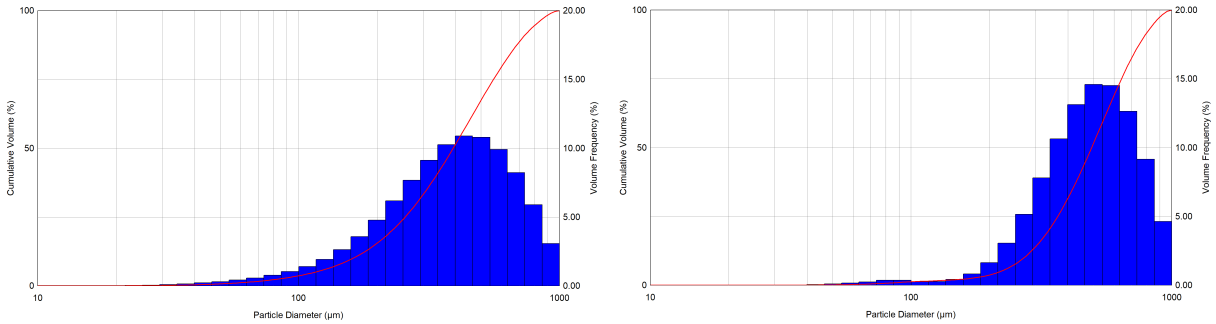

Figure 10: Comparison of droplet size distribution between left (water/water injection) and right (mixture/water injection)

5. Conclusion

Only few design guidelines for liquid-liquid pintle injectors in rocket engines are available in open literature. In the past, pintle injectors have been successfully used in throttleable thrusters, but with new propellants also new challenges rise. This study emphasizes the challenges of designing pintle injectors for new green hypergolic propellant combinations like HIP_11. A liquid-liquid pintle injector has been developed to screen the influence of high viscosity on spray behaviour in cold flow tests with simulants. Insights into the C_d-values could be achieved. Additionally, the throttling of the inner fluid through the outer fluid stream was visible. Even at low injection pressures and velocities, a hollow spray cone was formed. As expected, the spray cone from the mixture/water injection was much coarser than with water/water injection. The comparison of the shadowgraph images showed no significant influence of the fuel simulants viscosity on the spray cone angle. Furthermore, droplet size measurements quantified the visual observance that with mixture/water injections the droplets are bigger than with only water/water injections. The injector is the first iteration in the development line. More tests with different injector geometries will be conducted. During injector design special attention was paid to the possibility to transfer the fluid flow conditions to the development for hot firing injectors and also movable pintle injectors later on.

DOI: 10.13009/EUCASS2023-637

6. Acknowledgments

The authors would like to thank the DLR machine shop for manufacturing the injector parts. Special thanks to the colleges from DLR test bench M11 for the support in building the cold flow test bench.

References

[1] M. J. Casiano, J. R. Hulka, and V. Yang. "Liquid-Propellant Rocket Engine Throttling: A Comprehensive Review". In: *Journal of Propulsion and Power* 26.5 (2010), pp. 897–923. DOI: 10.2514/1.49791.

[2] G. Dressler and J. Bauer. "TRW pintle engine heritage and performance characteristics". In: *36th AIAA/ASME/SAE/ASEE Joint Propulsion Conference and Exhibit*. Reston, Virigina: American Institute of Aeronautics and Astronautics, 2000. DOI: 10.2514/6.2000-3871.

[3] M. Negri and F. Lauck. "Hot Firing Tests of a Novel Green Hypergolic Propellant in a Thruster". In: *Journal of Propulsion and Power* 38.3 (2022), pp. 467–477. DOI: 10.2514/1.B38413.

[4] F. Lauck, J. Balkenhohl, M. Negri, D. Freudenmann, and S. Schlechtriem. "Green bipropellant development – A study on the hypergolicity of imidazole thiocyanate ionic liquids with hydrogen peroxide in an automated drop test setup". In: *Combustion and Flame* 226 (2021), pp. 87–97. DOI: 10.1016/j.combustflame.2020.11.033.

[5] N. Ashgriz. *Handbook of Atomization and Sprays*. Boston, MA: Springer US, 2011. DOI: 10.1007/978-1-4419-7264-4.

[6] P. Cheng, Q. Li, S. Xu, and Z. Kang. "On the prediction of spray angle of liquid-liquid pintle injectors". In: *Acta Astronautica* 138 (2017), pp. 145–151. DOI: 10.1016/j.actaastro.2017.05.037.

[7] T. Yuan, C. Chen, and B. Huang. "Optical Observation for the Impingements of Nitrogen Tetroxide/Monomethylhydrazine Simulants". In: *AIAA Journal* 44.10 (2006), pp. 2259–2266. DOI: 10.2514/1.18375.

[8] W. C. Schumb, C. N. Satterfield, and R. L. Wentworth. *Hydrogen peroxide*. REINHOLD PUBLISHING CORPORATION, 1955.

[9] A. Volk and C. J. Kähler. "Density model for aqueous glycerol solutions". In: *Experiments in Fluids* 59.5 (2018). DOI: 10.1007/s00348-018-2527-y.

[10] N.-S. Cheng. "Formula for the Viscosity of a Glycerol−Water Mixture". In: *Industrial & Engineering Chemistry Research* 47.9 (2008), pp. 3285–3288. DOI: 10.1021/ie071349z.

[11] C. Bell and Contributors. *Thermo: Chemical properties component of Chemical Engineering Design Library (ChEDL)*. 2016-2021. URL: https://github.com/CalebBell/thermo,(retrieved:30.06.2023).

[12] E. W. Lemmon, I. H. Bell, M. L. Huber, and M. O. McLinden. "Thermophysical Properties of Fluid Systems". In: *NIST Chemistry WebBook, NIST Standard Reference Database 69*. Ed. by P. Linstrom. National Institute of Standards and Technology. URL: https://doi.org/10.18434/T4D303,(retrieved:30.06.2023).